JCTC Journal of Chemical Theory and Computation

Article

Cite This: J. Chem. Theory Comput. 2018, 14, 3298−3310

pubs.acs.org/JCTC

Intrinsic Conformational Preferences and Interactions in α-Synuclein Fibrils: Insights from Molecular Dynamics Simulations

Ioana M. Ilie,[*,†,‡,¶] Divya Nayar,[§] Wouter K. den Otter,[†,‡,∥] Nico F. A. van der Vegt,[*,§] and Wim J. Briels[*,†,⊥]

[†]Computational Chemical Physics, Faculty of Science and Technology, University of Twente, 7500 AE Enschede, the Netherlands

[‡]MESA+ Institute for Nanotechnology, 7500 AE Enschede, the Netherlands

[¶]Department of Biochemistry, University of Zürich, 8057 Zürich, Switzerland

[§]Eduard-Zintl-Institut für Anorganische und Physikalische Chemie, Center of Smart Interfaces, Technische Universität Darmstadt, 64287 Darmstadt, Germany

[∥]Multi Scale Mechanics, Faculty of Engineering Technology, University of Twente, 7500 AE Enschede, the Netherlands

[⊥]Forschungszentrum Jülich, ICS-3, D-52428 Jülich, Germany

Supporting Information

ABSTRACT: Amyloid formation by the intrinsically disordered α-synuclein protein is the hallmark of Parkinson's disease. We present atomistic Molecular Dynamics simulations of the core of α-synuclein using enhanced sampling techniques to describe the conformational and binding free energy landscapes of fragments implicated in fibril stabilization. The theoretical framework is derived to combine the free energy profiles of the fragments into the reaction free energy of a protein binding to a fibril. Our study shows that individual fragments in solution have a propensity toward attaining non-β conformations, indicating that in a fibril β-strands are stabilized by interactions with other strands. We show that most dimers of hydrogen-bonded fragments are unstable in solution, while hydrogen bonding stabilizes the collective binding of five fragments to the end of a fibril. Hydrophobic effects make further contributions to the stability of fibrils. This study is the first of its kind where structural and binding preferences of the five major fragments of the hydrophobic core of α-synuclein have been investigated. This approach improves sampling of intrinsically disordered proteins, provides information on the binding mechanism between the core sequences of α-synuclein, and enables the parametrization of coarse grained models.

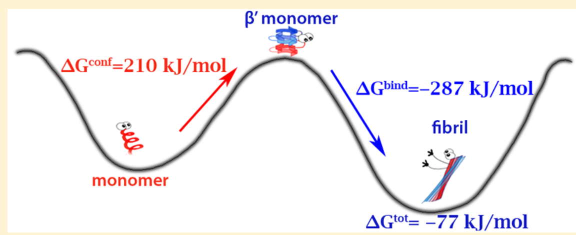

INTRODUCTION

The accumulation of amyloid fibrils is the hallmark of many neurodegenerative disorders, such as Parkinson's disease and Alzheimer's disease.[1,2] The proteins associated with these disorders, α-synuclein and the amyloid-β peptide, are known to adapt their conformations and aggregate into higher order insoluble aggregates such as oligomers and amyloid fibrils found in the brains of unhealthy patients.[3−8] Amyloids are characterized by a cross-β-sheet arrangement of proteins consisting of arrays of β-sheets running parallel to the long axis of the fibrils.[9−12]

The formation of fibrillar structures is kinetically described by a nucleation and elongation mechanism.[13,14] The nucleation phase represents the time that is required for a stable protein nucleus to form, which can then act as a template for the free monomers in solution.[3] During this phase the proteins undergo conformational changes and rearrange into monomer absorbing ordered aggregates. While nucleation is a rare event, elongation is a much faster process that occurs through monomer binding at fibrillar ends.[14] The growth process of an amyloid fibril has been suggested to manifest two phases: "stop and go".[15−18] A growth period during which free monomers simply attach at both ends of a fibril ("go") interrupted by long pauses during which monomer attachment is hindered ("stop").

Various experimental and simulation techniques have been used to understand and explain fibrillar growth. The growth of a fibril is a complex process that extends beyond nucleation and elongation: in many cases primary nucleation, elongation, secondary nucleation, and fragmentation contribute to the evolution of monomers toward an amyloid fibril.[3,14,19] Furthermore, the irregular elongation of the fibril is characterized by multiple elongation rates[15,20] and attachment free energies.[21] Some of these processes extend beyond the resolution of experimental methods; hence their microscopic understanding requires a different approach.

Computer simulations represent a powerful and complementary tool to capture and explain properties and phenomena that occur on time and length scales where experiments do not have enough resolution.[22,23] A promising computational method is to study fibrillar growth by coarse grained models. In the ideal representation, proteins are described as single

Received: February 19, 2018
Published: May 1, 2018

DOI: 10.1021/acs.jctc.8b00183
J. Chem. Theory Comput. 2018, 14, 3298−3310

particles able to adapt functionality as a function of the environment, representing the agility of amyloid-forming proteins.[24−26] These models predicted the formation of a critical nucleus of four monomers for fibril formation[26] and provided insight into the aggregation pathways, either through direct growth of fibrils or via oligomeric intermediates.[24,25] Furthermore, the one particle models showed that a fibril can act as a catalyst that enhances the transformation of an oligomer into a fibril[24] and reproduced the multistep growth process including secondary nucleation and fragmentation.[27] Models using a few particles per protein were successfully used to differentiate between amyloid-forming and amyloid-protected states and to analyze the formation of distinct oligomer and fibril morphologies, by various thermodynamically or kinetically selected pathways.[28,29] Fibril elongation hampered by multiple short arrested states was observed in a multiparticle chain model.[30]

The coarse grained models are highly efficient but unable to provide microscopic information into the exact folding mechanisms or quantitatively reproduce the structural heterogeneity of intrinsically disordered proteins. Atomistic simulations provide detailed information on the structural properties, the folding process, and the binding affinities of peptides but are still limited due to the many states in which a system can be. The most investigated intrinsically disordered protein is amyloid-β responsible for Alzheimer's disease. It is a fairly small protein of 42 amino acids, making it an ideal candidate for atomistic simulations in explicit solvent. Conformational preferences[31−33] as well as structural details of the fibrillar core[33,34] or interactions with membranes[35] have been investigated for the amyloid-β peptide. The complexity, length, and intricacy of α-synuclein, the 140 amino acid protein implicated in Parkinson's disease, make it difficult to study it as a whole at the full atomistic level for long time scales. Since the hydrophobic core is the building block of α-synuclein fibrils, many atomistic studies are limited to truncated or mutated fragments of the protein[36−38] or to simulating on relatively short time scales.[39] Studies mainly focus on the importance of the solvent or the pH on the conformational ensemble[40,41] and long-range interactions between the N- and C-terminal regions of the protein.[42]

Exploring the conformational free energy landscape of the full α-synuclein protein requires high computational power due to its conformational flexibility. α-Synuclein, also known as the "protein chameleon",[4] has the ability to adapt its secondary structure in response to the environment.[4,43] It can adopt an α-helical conformation upon binding to membranes,[44,45] it forms the characteristic in-register arrangement of β-sheets in fibrils,[46] and it is mainly unstructured in solution. The central ~60 amino acids play a key role in fibril formation and represent the building block of amyloids.[46] The conformational free energy landscape and binding contributions to β-strand stabilization of the five main fragments in the core region have, to our knowledge, not been quantitatively investigated by molecular dynamics simulations in explicit water, nor are they fully understood. Starting from the solid state NMR structure of an α-synuclein fibril,[47] we isolate the individual β-strands of the fibrillar core to characterize their contribution to fibril stability. In this study, we investigate the conformational preference of the individual α-synuclein fragments that play a key role in amyloids. Furthermore, we report the binding preferences of the individual strands and characterize the separate contributions of hydrogen bonds and hydrophobic interactions. This aids in understanding the mechanisms behind fibril stability and provides the necessary information to parametrize coarse grained models specifically aimed at α-synuclein aggregation.[30]

■ THEORY AND METHODS

System Preparation. The aim of the present study is to dissect and characterize the individual components of the core of an α-synuclein fibril and examine their contributions to fibril growth and stabilization. The fragments have been extracted from the solid state NMR structure of the orthogonal Greek key topology of an α-synuclein filament (PDB ID 2N0A).[47] The individual fragments are highlighted in Figure 1 by the different letters and colors:

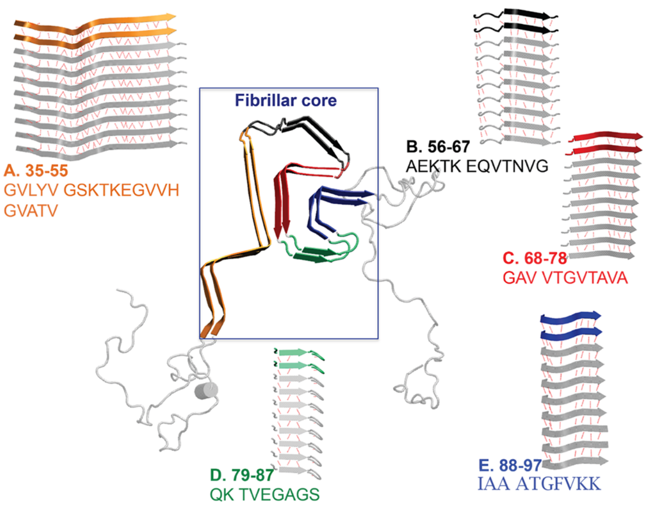

Figure 1. Solid state NMR structure of the orthogonal Greek key topology of an α-synuclein protein (PDB ID: 2N0A[47]). The extracted fragments are highlighted in 35−55 (A, orange), 56−67 (B, black), 68−78 (C, red), 79−87 (D, green), and 88−97 (E, blue). This color scheme is maintained throughout the paper.

(A) 35−55 (EGVLYVGSKTKEGVVHGVATV) in orange,
(B) 56−67 (AEKTKEQVTNVG) in black,
(C) 68−78 (GAVVTGVTAVA) in red,
(D) 79−87 (QKTVEGAGS) in green and
(E) 88−97 (IAAATGFVKK) in blue.

Each sequence corresponds to a single β-strand from the orthogonal Greek topology fibril (further referred to as β'-structure) that participates in β-sheet formation.

We carry out three sets of simulations: first, Metadynamics simulations of five monomeric systems containing a single fragment (A through E) in solution to characterize the internal conformational preferences of the fragments; second, umbrella sampling simulations on five dimeric systems containing two identical fragments (AA through EE, the highlighted pairs in Figure 1) to determine the hydrogen bonding interaction contributing to the stability of fibrils; third, umbrella sampling simulations on two dimeric systems to establish the hydrophobic interactions between unlike fragments (AC and CE) in a fibril.

Simulation Protocol. The simulations were carried out using the GROMACS 4.6.7 and the GROMACS 2016.1 simulation packages[48−50] for the conformational sampling and the determination of the binding energies, respectively. All simulations were performed using the all-atom CHARMM27/

DOI: 10.1021/acs.jctc.8b00183
J. Chem. Theory Comput. 2018, 14, 3298−3310

CMAP force field[51,52] and the TIP3P water model.[53] The N- and C-termini of all fragments were capped with acetyl and *N*-methylacetamide groups, respectively, using VMD.[54] All systems were maintained at constant temperature and pressure of 300 K and 1 bar, respectively, by using the modified Berendsen thermostat[55] and the Parrinello−Rahman barostat.[56] The temperature and pressure coupling times were fixed to 0.1 and 2 ps, respectively. For the conformational sampling, the short-range interaction cutoff was set at 1.2 nm, whereas for sampling of binding energies, it was set at 1.4 nm. The potential smoothly converges to zero at the cutoff using the Verlet cutoff scheme.[48−50] The long-range dispersion correction was applied for pressure and energy. The Particle Mesh Ewald (PME) technique[57] with a cubic interpolation order, a real space cutoff of 1.2 nm (conformational sampling) or 1.4 nm (binding interactions), respectively, and a grid spacing of 0.16 nm was employed to compute the long-range electrostatic interactions. Bond lengths were constrained by means of a fourth order LINCS algorithm with 2 iterations.[58] In all simulations, the time step was fixed to 2 fs, and periodic boundary conditions were applied. The positive charges of the E fragment were neutralized by replacing water molecules with Cl^- ions. The five monomeric systems were each solvated in 16905, 4501, 4359, 2884, and 2848 water molecules in cubic boxes. The dimeric systems were solvated in triclinic boxes elongated along the *z*-axis containing 46875, 11251, 7779, 5443, and 7816 water molecules for the five hydrogen bonding systems and 14308 and 11111 water molecules for the hydrophobic systems, respectively. Energy minimization of the systems was followed by temperature equilibration at 300 K for 0.5 and 2 ns, respectively, and pressure equilibration at 1 bar. Simulations were performed at constant *NPT* with snapshots saved every 5 ps over a total run length of 300 ns for the conformational sampling (600 ns for the 35−55 fragment) and 200 ns for the binding sampling.

Metadynamics. One aim of the present study is to characterize the conformational preferences of the individual fragments involved in β-sheet formation, which is achieved using Metadynamics, an enhanced sampling technique that allows one to reconstruct the multidimensional free energy landscapes of complex systems.[59−62] The main idea behind Metadynamics is to bias the dynamics of a system by a history dependent potential, V_G, constructed in the space of a set of collective variables (CVs), **S**. This potential consists of the sum of repulsive Gaussians deposited along the trajectory of the collective variables with the aim to prevent the system from returning to a configuration that has already been sampled. The CVs are a set of *n* functions of the microscopic coordinates of the system **Q**, $\mathbf{S}(\mathbf{Q}) = (S_1(\mathbf{Q}), S_2(\mathbf{Q}), ..., S_n(\mathbf{Q}))$. The bias potential at time t is described by[59]

$$V_G(\mathbf{S}, t) = \omega \sum_{i=1}^{t/\tau} \exp\left\{-\frac{[\mathbf{S} - \mathbf{S}(i\tau)]^2}{2\sigma^2}\right\} \quad (1)$$

with τ being the deposition interval, ω the height, and σ the width of the Gaussians deposited along the CVs. After a sufficiently long simulation time, all configurations in CV space have been sampled (the potential grows approximately linearly in time) and the free energy landscape of the system can be estimated by $A(\mathbf{S}) \propto -\lim_{t\to\infty} V_G(\mathbf{S}, t)$.

An important aspect in Metadynamics is the choice of the collective variables. In order to efficiently describe the system, they must clearly differentiate between the different states a system can adopt. When dealing with intrinsically disordered proteins, multiple states can become mapped on the same set of values of the collective variables. The conformations of a protein are best characterized in terms of the dihedral angles ϕ and ψ, denoting the angle about the C_α−N and C_α−C_O bonds, respectively. The peptides discussed here consist of several amino acids and would require as many pairs of dihedral angles. This large set of CVs is computationally too expensive, and the free energy landscape would require a long time to converge. It is computationally feasible and physically reasonable to describe a polypeptide via linear combinations of the deviations of the dihedral angles from their values ϕ_i^{ref} and ψ_i^{ref} in a reference structure. With this in mind, two AlphaBeta collective variables, S_1 and S_2, were chosen such that

$$S_1 = \frac{1}{2}\sum_{i=1}^{N}[1 + \cos(\phi_i - \phi_i^{\mathrm{ref}})]$$
$$S_2 = \frac{1}{2}\sum_{i=1}^{N}[1 + \cos(\psi_i - \psi_i^{\mathrm{ref}})] \quad (2)$$

with *N* being the number of amino acids in the peptide chain, and the solid state NMR structure of an α-synuclein protein[47] was chosen as reference. For small deviations from the reference structure, the collective variables will have a maximum value of $S_{\max} = N$, while the CVs lose their structural specificity for larger deviations from the reference structure with the minimum values of zero. PLUMED2.0[63] was used to deposit the Gaussians every 1 ps, with a height of $\omega = 0.2$ kJ/mol and a width of $\sigma = 0.3$.

Umbrella Sampling. To determine the inter- and intramolecular binding energies of α-synuclein β' fragments, we use umbrella sampling.[64−66] The main idea is to add a harmonic bias to the potential to ensure efficient sampling along a chosen reaction coordinate of states otherwise hardly accessible. Two protein fragments were extracted from the solid state NMR fibrillar structure. The distance between their centers of mass, *d*, is used as the reaction coordinate. Following the simulation protocol of umbrella sampling, the range of *d* is divided into several "windows" centered at values d_i. The harmonic bias potential $\omega_i(d)$ restricts the system in the *i*th window to fluctuate around d_i by

$$\omega_i(d) = \frac{1}{2}K(d - d_i)^2 \quad (3)$$

with the force constant $K = 1000$ kJ/(mol nm^2). The net effect of the bias potential is to connect energetically separated regions in phase space[66] by changing the total energy of the system into $E_i^{\mathrm{b}} = E^{\mathrm{u}} + \omega_i(d)$, with *E* being the energy and the corresponding superscripts denoting the biased and the unbiased quantities, respectively. The unbiased free energy for window *i* is calculated based on the biased probability distributions P_i^{b} and the bias potential,

$$A_i(d) = -k_B T \ln P_i^{\mathrm{b}}(d) - \omega_i(d) + f_i \quad (4)$$

with f_i being a window-dependent offset. The windows are then combined into a single free energy curve by using the weighted histogram analysis method (WHAM)[67] to determine the values of the constants f_i.

To improve the sampling efficiency, both fragments are restricted to sample β' configurations only. This is realized by position restraining the backbone of the fragment closest to the

DOI: 10.1021/acs.jctc.8b00183
J. Chem. Theory Comput. 2018, 14, 3298−3310

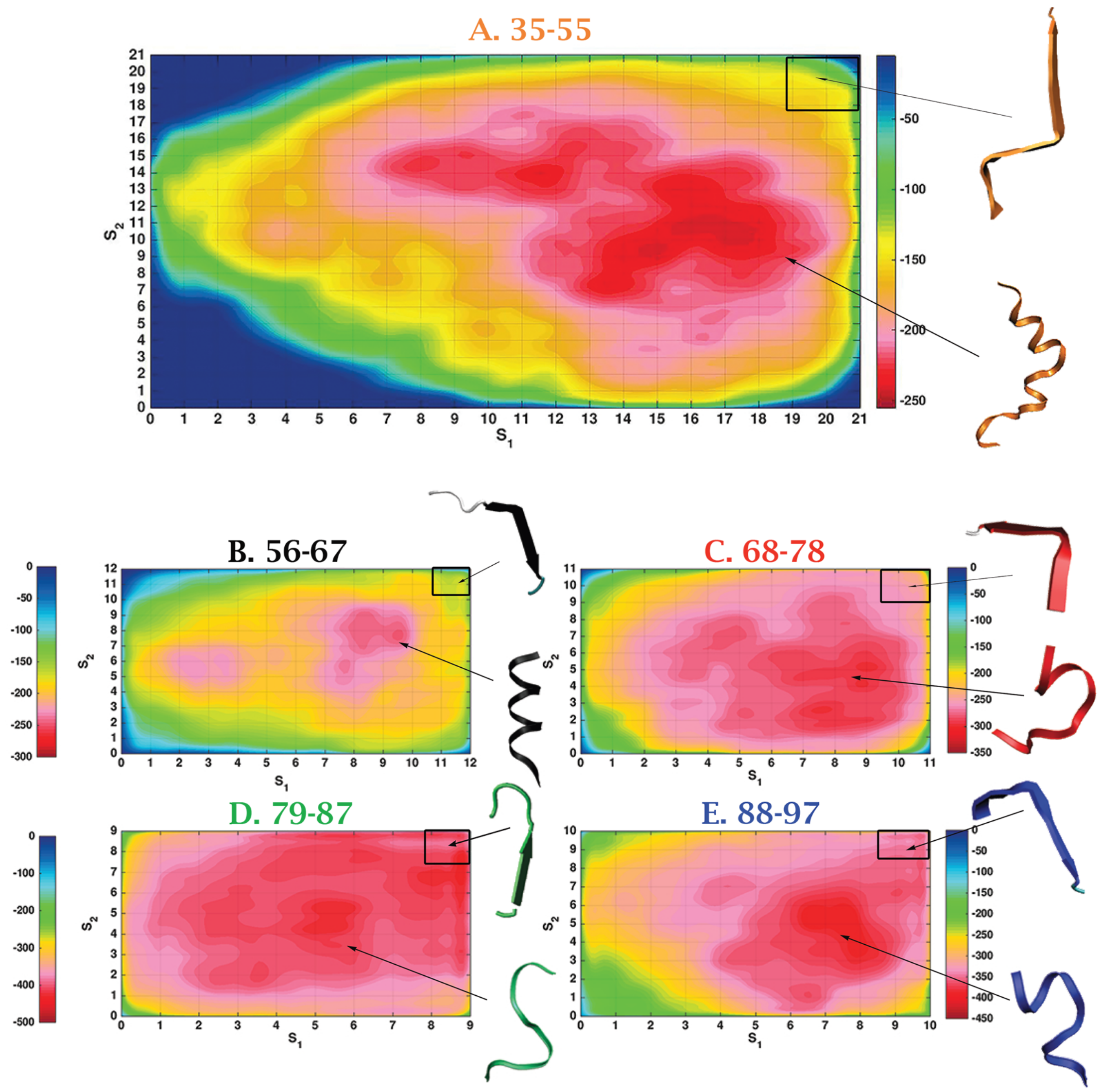

Figure 2. Free energy surface as a function of the collective variables S_1 and S_2 for the fragments building the fibrillar core of an α-synuclein fibril. The residue numbers constituting every fragment are displayed in the title of every plot. The snapshots show representative conformations for the highlighted regions. The free energy scale is in kJ mol^{-1}.

N-terminus of the protein and by restraining the dihedral angles in the backbone of the other fragment. In both cases harmonic restraints with force constants of 1000 kJ/(mol·nm^2) for the positions and 1000 kJ/(mol·rad^2) for the dihedrals were applied using the solid state NMR β' configuration as the reference state. The initial configurations were prepared by placing the two fragments with the long axes of their backbone β-strands oriented parallel. For the hydrogen-bonding simulations, the two strands were oriented to form a β-sheet; for the hydrophobic simulations, the planes of the strands were facing each other, in both cases realizing orientations akin to those occurring in the fibril, see Figure 1. At $d = 0$, the centers of mass of the fragments coincide; initial configurations at larger values of d were generated by moving the configuration restrained protein away from the position-restrained protein, perpendicular to the long axis of the position-restrained protein. The simulation windows were generated for center of mass distances up to 2.5 nm, with a step of 0.1 nm. Every window was simulated under constant NPT conditions for about 200 ns where the first 2 ns were considered to be part of the pressure equilibration phase.

■ RESULTS

Conformational Preferences. To characterize the contributions of the individual strands to fibril formation, we started by decoupling the conformational degrees of freedom from the interactions between different strands. As a first step, we analyze the conformational free energy landscape of the fragments as a function of the collective variables S_1 and S_2 as shown in Figure 2. The convergence of these simulations with increasing run time is illustrated in Figure S1. All fragments show rugged free energy landscapes characterized by multiple local minima. This lack of a dominant global minimum surrounded by high energy barriers is a common feature of intrinsically disordered proteins.[68] Every minimum corresponds to a different conformational state sampled by the biased simulation. Representative structures are highlighted in the snapshots next to each free energy surface. The snapshots from the upper right corners of the free energy plots correspond to

DOI: 10.1021/acs.jctc.8b00183
J. Chem. Theory Comput. 2018, 14, 3298−3310

the fibrillar β' structures. The β-rich arrangements do not display any specific minima in the free energy plots despite the fact that they are sufficiently sampled by the Metadynamics simulations. The snapshots in the lower right corner of each free energy plot, Figure 2, show representative, yet not unique, conformations that the fragments can adopt.

To characterize the transitions between β'- and non-β'-structures, we calculated the free energy difference, $\Delta G_{\beta',1-\beta'}$, between the two states:

$$\exp[-\Delta G_{\beta',1-\beta'}(\Delta S)/RT] = \frac{\iint_{\beta'} e^{-A(S_1,S_2)/RT}\, dS_1 dS_2}{\iint_{1-\beta'} e^{-A(S_1,S_2)/RT}\, dS_1 dS_2} \tag{5}$$

where S_1 and S_2 in the integrals over β' run from $N - \Delta S$ to N while the integrals over $1 - \beta'$ run over all the non-β' states. To determine the optimal value of ΔS, we opted for square regions of the configuration space $\Delta S_1 = \Delta S_2 = \Delta S$. The computed $\Delta G_{\beta',1-\beta'}$ as a function of the value of ΔS for all five fragments are shown in Figure 3. The initial rapid decrease of $\Delta G_{\beta',1-\beta'}$ for

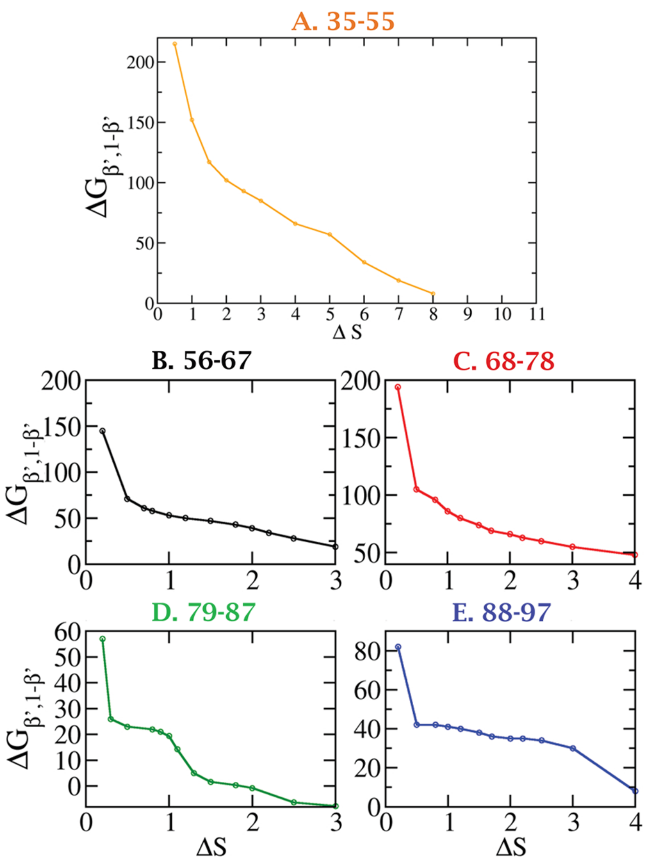

Figure 3. Free energy difference $\Delta G_{\beta',1-\beta'}$ between the β'- and non-β'-structures as a function of ΔS calculated from eq 5 for all five fragments.

$\Delta S \leq 0.5$ indicates that the integral in the numerator in eq 5 does not yet encompass the entire free energy minimum associated with the β' conformation for these low values of ΔS. The decay levels off beyond $\Delta S = 0.5$, but fragments A, B, and C do not show the clear plateau in the free energy that is required for a well-defined separation of β' and non-β' conformations. The steady decline of the free energy with ΔS indicates that the β' configuration is not stable in solution. To obtain a reasonable value for ΔS, we therefore next turn our attention to structural details.

To further examine the extent of the β' structure in S_1 and S_2 space, we isolated and analyzed separately every minimum by studying conformational properties of the fragments. We examined the Ramachandran plots and other observables such as root mean squared deviations from the solid state NMR and radii of gyration. The most revealing information is given by the deviations $\Delta\phi$ and $\Delta\psi$ of the dihedral angles ϕ and ψ from their corresponding reference values in the β'-state, ϕ_i^{ref} and ψ_i^{ref}, respectively. The dihedral deviations shown in Figure 4 for fragment C were calculated by extracting from the Metadynamics simulations all configurations with CVs within the choice of ΔS, followed by unbiasing.[62,69] These values correspond to squares of area ΔS^2 in the upper right corners of the unbiased free energy landscape of fragment C in Figure 2. For $\Delta S = 1$, little deviation from the β' dihedral angles is observed, as evident from the presence of a single large peak in Figure 4a. The Ramachandran plot aimed specifically at the same subspace of the free energy plot confirms that mainly β-rich states are being sampled (Figure S2). With increasing ΔS, upon enlarging the subspace, various other states are being sampled. For $\Delta S = 3$, the peak widens considerably and its maximum shifts toward $\Delta\phi = -60°$, and a secondary peak emerges at $\Delta\phi = \Delta\psi = 60°$, giving rise to different secondary structures such as polyproline II helix and various α-helices. A further increase to $\Delta S = 4$ leads to the development of multiple other peaks, which correspond to α-helical structures. The other fragments show similar behavior, as can be seen in Figures S3−S6 in the Supporting Information. We will return below to the numerical choice of ΔS.

Interplay of Interactions in Fibril Formation. The complex interplay between conformational preference, hydrogen bonding, hydrophobic interactions, salt bridges etc. lies at the heart of amyloid formation. Having characterized the fragments from a conformational point of view, the next natural step is to investigate the influence of the interactions on fibril formation and stabilization. We start by describing the hydrogen bonds (H-bonds) and then proceed with the hydrophobic interactions.

Hydrogen Bonding. To describe the importance of hydrogen bonds along the direction of fibrillar growth, we built five separate systems, each consisting of two identical protein fragments extracted from the solid state NMR structure corresponding to two different α-synuclein proteins, see the snapshots in Figure 1. The results from this analysis allow us to separately examine the contributions of each fragment to the hydrogen bonding interactions to form the fibril.

Figure 5 shows the free energy curves for all fragments as functions of the reaction coordinate, the center of mass to center of mass distance d. The snapshots highlight representative conformations at 0.5 nm and at larger distances together with hydrogen bonds formed between two fragments. The free energies mainly reflect the strength of the hydrogen bonds between two peptides, yet one should keep in mind that the interactions between the side chains also contribute. The plots in Figure 5 show a clear dependence of the curves' shapes and depths on structure and the number of amino acids in the fragments. Upon pulling two short fragments slightly apart, as for fragment D, they completely detach from each other, hence the single well-defined minimum in Figure 5D. The maximum number of hydrogen bonds formed between two D fragments is low because the β content of this fragment is low. Note that the

DOI: 10.1021/acs.jctc.8b00183
J. Chem. Theory Comput. 2018, 14, 3298−3310

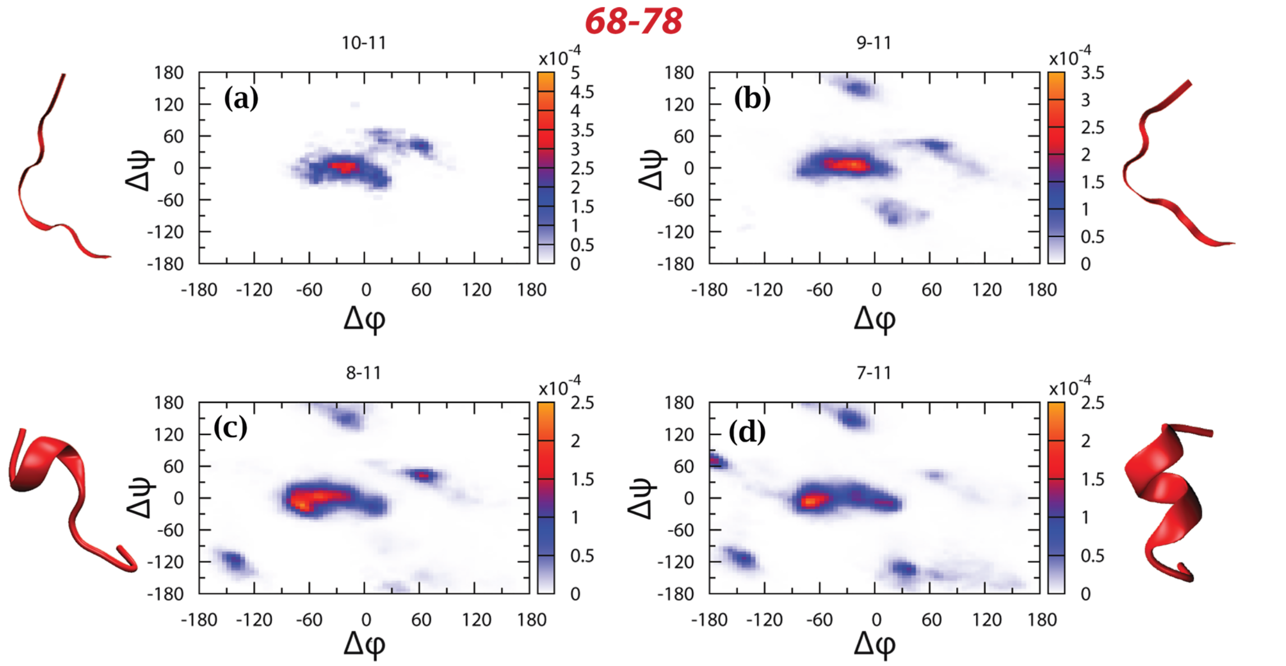

Figure 4. Normalized probability distributions of the dihedral angles for fragment C for (a) $\Delta S = 1$ and hence $\{S_1, S_2\} \in [10; 11]$, (b) $\Delta S = 2$, (c) $\Delta S = 3$, and (d) $\Delta S = 4$. The snapshots next to the plots show representative configurations of the C fragment.

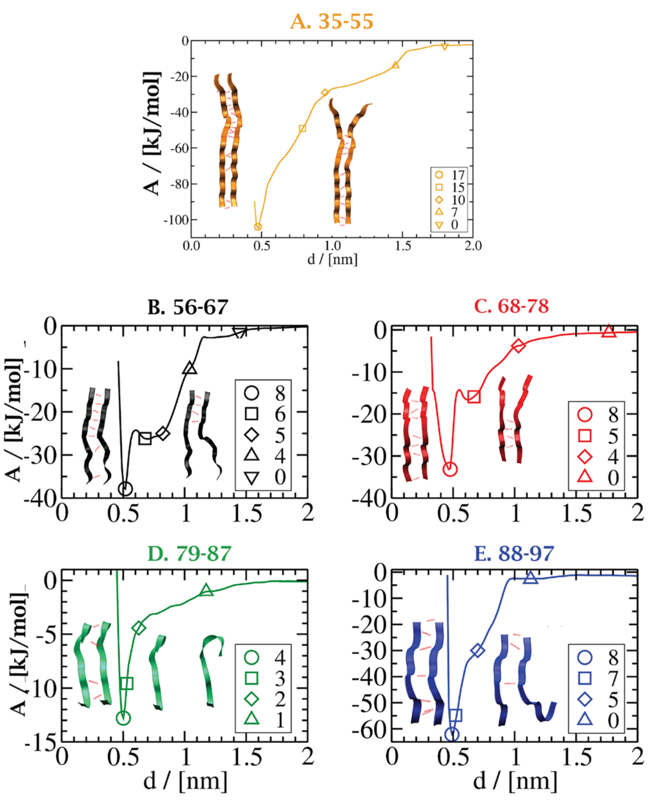

Figure 5. Free energy curves as a function of the center of mass distances between two identical protein fragments. The markers represent the average number of hydrogen bonds between the peptides' backbones at the given distances. Two atoms are considered to form a H-bond if the bond is unique, within a donor−acceptor (D−A) distance of 0.35 nm and within an angle cutoff (A−DH) of 30°. The snapshots show typical configurations at 0.5 nm and at larger distances. The H-bonds in the snapshots are highlighted by the red lines connecting the fragments.

last H-bond recorded is formed internally within a peptide despite the conformation restrictions. With increasing number of amino acids, the detachment becomes a more complex process. The free energy of the E fragment (blue curve) shows a deep minimum at the optimal attachment distance and a small ledge following the breaking of several hydrogen bonds at ∼0.7 nm. This small plateau widens as the number of residues in the fragment increases, as seen by comparing E with C and B. For these longer fragments, the detachment proceeds stepwise: at first about three hydrogen bonds break simultaneously, and the dimers are stabilized by the remaining five bonds. With increasing distance, these bonds break in rapid succession. Interestingly, the longest peptide (A) does not show an intermediate plateau but a fairly uniform rise of the free energy profile, suggesting a sequential breaking of the hydrogen bonds. Closer inspection reveals that the initial 17 hydrogen bonds still dissociate in steps of three to four hydrogen bonds with increasing distance, with the last seven bonds breaking simultaneously.

Interestingly the depth of the free energy curve of fragment E is lower than that for fragments B and C even though all three dimers are connected by a maximum of 8 hydrogen bonds. The E peptide is not only the most bent one but also the sole charged fragment. Here an additional contribution to the free energy arises from the electrostatic contribution due to the charges. Note that the optimal attachment (center of mass to center of mass) distance is at 0.5 nm for all dimers independent of the sequence structure. The shape of the free energy curves is mainly dictated by the length of the fragments, whereas the depth is mainly driven by hydrogen bonds with small contributions arising from van der Waals and electrostatic interactions. The contributions of each fragment to fibril stabilization arising from hydrogen bonding contributions are calculated by[30]

DOI: 10.1021/acs.jctc.8b00183
J. Chem. Theory Comput. 2018, 14, 3298−3310

$$\Delta G^{\mathrm{Hb}} = -RT \ln\left[\frac{4\pi d_0^{\ 2}}{Q(d_0)} c_0 \int_0^{d^\ddagger} Q(\bar{d})\, \mathrm{d}\bar{d}\right] \tag{6}$$

as derived in the Appendix. Here the partition function as a function of the distance is obtained from the simulations for small distances, $Q(d) = \exp[-A(d)/(RT)]$ and from the entropy-dominated extrapolation $Q(\bar{d}) = Q(d_0)\bar{d}^2/d_0^{\ 2}$ for distances beyond the interaction range. Here d_0 is an arbitrary distance (beyond the interaction range) used to merge the two partial solutions, $d^\ddagger$ location of the transition state of the binding reaction, R the gas constant, and c_0 a reference concentration typically taken as 1 M. As a consequence of the high transition states to the calculated functions $A_{i'i'}(\bar{d})$, implying low populations of the transition regions, the precise locations of the transition states $d^\ddagger$ are of little influence; we selected $d^\ddagger = 2.0$ nm for all fragments. This distance was also used as the reference d_0 in the evaluation of the long-distance distribution.

Numerical results on the detachment free energies are provided along the diagonal of Table 1. The A fragment has the largest stabilizing hydrogen bonding effect whereas the shortest peptide (D) has the least stabilizing effect.

Table 1. Free Energy Contributions (in kJ/mol) of Each Fragment to Fibril Formation and Stabilization[a]

	A	B	C	D	E	$\Delta G_{\beta',1-\beta'}$
A	−96		−2.5			106
B		−38				39
C	−2.5		−33		−2.5	30
D				−14		0
E			−2.5		−60	35
connectivity			−41			0
total			≈ −287			**210**

[a]The $\Delta G_{\beta',1-\beta'}$ values are reported for $\Delta S = 2$. The diagonal elements represent hydrogen bonding between like fragments, the off-diagonal elements represent hydrophobic interactions between unlike fragments, and the last column represents conformational free energies for $\Delta S = 2$. The "connectivity" contribution is discussed in the main text and derived in the Appendix. The two totals refer to the binding and conformational free energies, respectively.

Hydrophobic interactions. To measure the strength of the hydrophobic interaction, we extracted the fragments A, C, and E from the solid state NMR structure. Following the procedure described in the Umbrella Sampling section, in the first set of simulations, the C fragment was kept fixed through position restraints, and the configuration restrained E peptide was sampled at a series of intersegmental center of mass distances. In the second set of simulations, the A fragment was for computational reasons reduced to the part that interacts with C, that is, residues 48−55. This truncated A fragment was position restrained, and the configuration restrained C peptide was sampled at various distances. The calculated free energies are shown in Figure 6a,b, with snapshots highlighting the representative fragments chosen for analysis. The hydrophobic contributions are small relative to the hydrogen-bonding interactions; application of eq 6 yields $\Delta G^{\mathrm{hydrophobics}} = -10$ kJ/mol for both the AC interaction and the CE interaction.

DISCUSSION AND CONCLUSION

The growth of amyloidogenic α-synuclein fibrils is the hallmark of Parkinson's disease. Fibrillar structures develop through a nucleation and growth mechanism, and their evolution has been widely explored by both experimental and simulation techniques. Still little is known about the individual and collective contributions of the β-strands to fibril formation and stabilization. With this in mind, numerical simulations using enhanced sampling techniques have been carried out on the α-synuclein fragments that form the core of amyloid fibrils. The conformational stabilities and the binding affinities of each individual peptide fragment have been separately investigated. Molecular dynamics simulations with explicit solvent have been carried out on each individual fragment starting from its ideal β'-conformation as extracted from solid state NMR.[47] The simulations show rugged free-energy surfaces for all protein fragments, independent of their sequence length or hydrophobicity. The absence of free energy barriers is a common feature for intrinsically disordered proteins, but it has, to our knowledge, not been demonstrated at this level for α-synuclein before. Computational studies on the amyloid-β(1−42) peptide revealed that all possible secondary structure categories are being sampled, making it an intrinsically disordered protein with a heterogeneous tertiary ensemble.[70] Other studies have characterized populations of α-synuclein in terms of distinct order metrics but did not examine the conformational preferences of the individual fragments and their contributions to the stability of the protein.[71] The present study shows that individual fragments have a high preference toward non-β'-states. The ideal β'-rich conformations do not represent local minima in the free energy curves. The same preference for non-β' states was observed also in other studies on α-synuclein, tau,

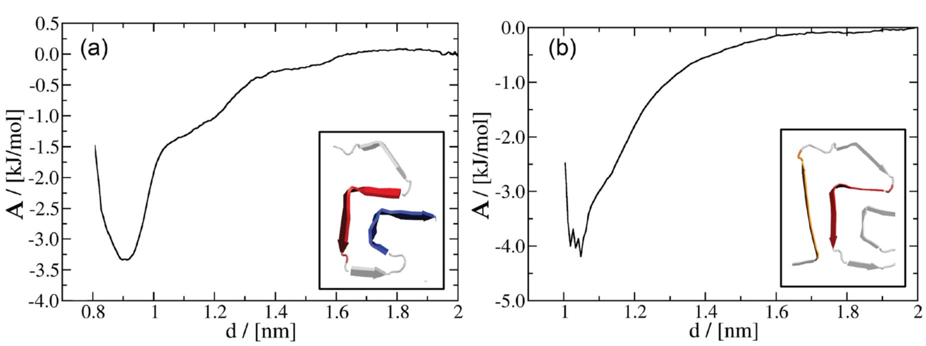

Figure 6. Free energy curves as a function of the center of mass distances between two protein fragments corresponding to the same protein. The snapshots highlight the three most hydrophobic fragments, which were chosen for analysis: the interactions of the C fragment in red with (a) the E fragment 88−97 in blue and (b) the second half of the A fragment in orange.

DOI: 10.1021/acs.jctc.8b00183
J. Chem. Theory Comput. 2018, 14, 3298−3310

and amyloid-β.[72,73] Studies on Alzheimer's amyloid-β peptide revealed that the conformations are dominated by loops and turns but show some helical structure in the C-terminal hydrophobic tail.[74] Furthermore, an increased α-helical content during fibrillogenesis of most amyloid-β peptides was reported.[75,76] The free energy landscape of Figure 2 suggests that fragments in solution are likely to adapt multiple conformations, including the helical conformation usually adapted by membrane-bound α-synuclein.[45,77]

Fibrillar structures are characterized by a high β-sheet content. The lack of any clear preference of the analyzed fragments toward this state indicates that external factors, that is, binding energies between fragments, compensate for the conformational loss in free energy. Dimers of conformationally restrained protein segments have been simulated to characterize the inter- and intraprotein interactions. The results suggest that the detachment depends on the length of the fragments as longer peptides undergo a stepwise detachment as compared to the abrupt disconnection observed for shorter fragments. A similar pattern was observed in a recent study on small fragments of the Aβ peptide and Sup35,[78] which showed that the growth and stability of fibrils depends on the peptide sequence.

The conformational free energies of the fragments, $\Delta G^{i}_{\beta',1-\beta'}$, the hydrogen bonding free energies of the five pairs of like fragments in their β' configurations, $\Delta G^{\mathrm{Hb}}_{i'i'}$, and the hydrophobic binding energies between the two analyzed pairs of unlike fragments in their β' configurations, $\Delta \tilde{G}^{\mathrm{hydrophobics}}_{i'C}$, based on the free-energy profiles in the Results section, are collected in Table 1. The total free energy change associated with a randomly coiled truncated α-synuclein in solution binding to an existing fibrillar template, with the five fragments adopting β' conformations and binding to the fibril's β-sheets, is calculated as

$$\Delta G^{\mathrm{tot}} = \sum_{i} \Delta G^{i}_{\beta',1-\beta'} + \sum_{i'} \Delta G^{\mathrm{Hb}}_{i'i'} + \sum_{i=A,E} \Delta \tilde{G}^{\mathrm{hydrophobics}}_{iC} + \Delta G^{\mathrm{connectivity}} \tag{7}$$

The connectivity term, derived in the Appendix, corrects for the five fragments being connected into a single protein. A single i' fragment in the β' configuration loses translation and rotation entropy upon binding to a fibril, which is included in the calculated values of $\Delta G^{\mathrm{Hb}}_{i'i'}$. But the sum of the entropy losses of five separate segments binding to a fibril differs from the entropy loss of a single chain of five fragments binding to a fibril: the five separate segments in solution move independently and therefore collectively possess more entropy than a single chain of five segments permanently moving together. The corresponding correction in the above expression for the free energy of a protein attaching to a fibril is calculated in the Appendix as $\Delta G^{\mathrm{connectivity}} \approx -41$ kJ/mol. The free energies $\Delta G^{\mathrm{hydrophobics}}$ of the two hydrophobic interactions cannot simply be added to this expression, as it would reintroduce double counting of the entropy loss. Hence, we derive in the Appendix an equation to approximate the contributions, $\Delta \tilde{G}^{\mathrm{hydrophobics}}$ to the overall binding free energy, which based on the umbrella sampling simulations yield values of approximately -2.5 kJ/mol for both AC and CE. As discussed in the Results section, the conformational free energies $\Delta G^{i}_{\beta',1-\beta'}$ are susceptible to the definition of the β' configuration, that is, the selection of ΔS. The values in Table 1 correspond to $\Delta S = 2$, which emerged from the previous discussion as a reasonable estimate. Equation 7 then yields a binding contribution $\Delta G^{\mathrm{bind}} = -287$ kJ/mol and a conformational contribution $\Delta G^{\mathrm{conf}} = 210$ kJ/mol, resulting in the total free energy change $\Delta G^{\mathrm{tot}} = -77$ kJ/mol indicating that binding is favorable. For comparison purposes, similar calculations with $\Delta S = 1$ and $\Delta S = 3$ are provided in the Supporting Information. The lower value raises the conformational free energy and renders ΔG^{tot} positive, that is, the protein will not bind to the fibril. The higher ΔS, however, lowers the conformational free energy and thereby promotes binding. We note that the free energy of two proteins in solution binding to form a short fibril of two proteins is readily obtained by double counting the configurational free energies in eq 7. The resulting values are positive for the two smaller values of ΔS, indicating that these short fibrils are unstable, while for the unrealistically large $\Delta S = 3$ the value is slightly negative. A fibril of n proteins is stable when the $n - 1$ binding free-energy gains between proteins outweigh the n conformational free-energy losses or $(n - 1)\Delta G^{\mathrm{bind}} + n\Delta G^{\mathrm{conf}} < 0$, which for $\Delta S = 2$ requires $n \geq 4$ while for $\Delta S = 1$ this break-even point is never reached. This indicates that the formation of a fibril nucleus is a rare event involving multiple proteins, even when addition of a single protein to an existing stable fibril is thermodynamically favorable.

The overall contributions per fragment to the free energy, that is, the sum of $\Delta G^{\mathrm{Hb}}_{i'i'}$ and $\Delta G^{i}_{\beta',1-\beta'}$, reveal the largest negative free energies for the D and E fragments, indicating that these two segments contribute the most to fibril stabilization. One may speculate that these fragments consequently also initiate binding of a protein to a fibril. The A fragment has the highest binding energy, but it loses more configurational free energy upon binding than any other. Assuming the connectivity term may be equally divided over the five fragments, only fragment A does not contribute to the binding. The hydrophobic contributions to the binding free energy appear to be relatively minor in the current study. It cannot be ruled out, however, that the collective hydrophobic effect of a multitude of fragments, for example, by shielding hydrophobic side groups in the center of a fibril or a multithread fibril from exposure to water, may have a more pronounced impact on the stability of an amyloid. Hydrophobic interactions are nonadditive for extended hydrophobic surfaces where the collective nature of interface formation breaks down the pair-additive assumption.[79] Such an effect was shown for other intrinsically disordered proteins such as human islet amyloid polypeptide and transthyretin.[80,81] The effect is nonlinear for short stacks of fragments but will of course become linear for longer arrangements. A more detailed exploration of this effect, requiring extensive simulations with a multitude of fragments, exceeds the objectives of the current study. With an improved evaluation of the hydrogen bonding contribution, the protein is likely to bind stronger and the total binding free energy is likely to be negative at smaller values of ΔS. The sum of all contributions, for $\Delta S = 2$, was calculated above as approximately -77 kJ/mol for the hydrophobic core of α-synuclein to attach to a fibril. This value compares favorably to the experimental value of -33 kJ/mol for the full protein.[21] The difference is attributed to the omission of the N- and C-terminal regions and the partial inclusion of the hydrophobic effect, as discussed above.

The result of this study aids in understanding the atomistic details of α-synuclein fibril stabilization, the importance of the

DOI: 10.1021/acs.jctc.8b00183
J. Chem. Theory Comput. 2018, 14, 3298−3310

individual components to the total free energy of a system as such, and parametrization of existing multiparticle coarse-grained models for α-synuclein[30] used to study fibrillar growth. The latter is a model developed to study the growth of an α-synuclein fibril by introducing a coarse representation of the protein. The hydrophobic core of the protein is represented as a chain of five "chameleon" particles[24,30] connected by springs (Figure S7). The interaction properties of these particles, representing the five fragments studied here, change in response to their environment, which affects the "configurations" of the particles.[24,30] This was realized by endowing the particles with internal "configuration" coordinates and internal potentials accounting for the configurational distributions of the fragments. These distributions, previously approximated as one-dimensional asymmetric double-well potentials (Figure S7d), can now be replaced by the two-dimensional free-energy surfaces of Figure 2. The interactions between the particles, which vary with their internal configuration coordinates, are to be replaced for the β'-configuration by the interaction free energies of Figures 3 and 5, after correction for the entropy sampled by mobile coarse-grained particles. We note that the hydrogen bonding interaction potential being used in ref 30 is actually close to that of the D segment. The heads and tails of the coarse-grained particles are connected by springs and thereby automatically include the connectivity correction derived in the Appendix. Besides these atomistic simulations, experimental data on the interfragment interactions will also be valuable in the parametrization of the coarse-grained model.

In conclusion, this study dissects the individual contributions of the β-strands of α-synuclein to fibril formation. Enhanced conformational sampling techniques have been employed to show that the individual β-strands in solution have a strong propensity for non-β structures, whereas the highly unstable fibrillar β'-rich state is stabilized in fibrils predominantly by hydrogen bonds and hydrophobic interactions. These interactions are expected to reduce the number of possible compact fibril conformations, constituting one of the driving forces of aggregation.[82] The association energies have been estimated and compared to experimental results. Furthermore, this study provides input for the parametrization of existing multiparticle coarse grain models for α-synuclein[30] and can assist experimental studies investigating the aggregation of truncated peptides.

■ APPENDIX: FREE ENERGY CALCULATION

The (un)binding reaction of a protein fragment, for example, a fragment of type A, with an identical fragment at the end of a fibril F can be described by the reactions

$$\mathrm{FA}' \rightleftharpoons \mathrm{F} + \mathrm{A}' \rightleftharpoons \mathrm{F} + \mathrm{A} \tag{8}$$

where A′ denotes a fragment in the β' state and A the fragment in solution. The equilibrium constant of the first reaction step is given by

$$K_{\mathrm{FA}'} = \frac{([\mathrm{FA}']/c_0)}{([\mathrm{F}]/c_0)([\mathrm{A}']/c_0)} = \exp\left[-\frac{\Delta G^\circ_{\mathrm{FA}'}}{RT}\right] \tag{9}$$

where the square brackets denote concentrations, c_0 is a reference concentration typically taken as 1 M, $\Delta G^\circ_{\mathrm{FA}'}$ is the standard free energy change of the reaction, and R is the gas constant. In statistical mechanics, this equilibrium constant is calculated as

$$K_{\mathrm{FA}'} = \frac{(q_{\mathrm{FA}'}/V)}{(q_{\mathrm{F}}/V)(q_{\mathrm{A}'}/V)}c_0 \tag{10}$$

where the q denote molecular partition functions in a volume V. In the dimeric simulation systems, the position-restrained fragment represents the fragment at end of the fibril, while the conformation-restrained fragment represents the fragment that (un)binds. The latter is considered bound if its distance $\overline{d}$ to the fibril's top-most A fragments is less than the separation at the transition state, $d^\ddagger$. With the fragment−fibril interaction being dominated by hydrogen bonding between the two like fragments, one obtains the partition function

$$q_{\mathrm{FA}'} = \alpha_{\mathrm{A}'}V\int_0^{d^\ddagger} Q_{\mathrm{A}'\mathrm{A}'}(\overline{d})\,\mathrm{d}\overline{d} \tag{11}$$

where $\alpha_{\mathrm{A}'}$ (dimension, m^{-3}) combines a number of elementary constants with fragment and fibril dependent parameters, and the distance-dependent partition function is related by

$$Q_{\mathrm{A}'\mathrm{A}'}(\overline{d}) = \exp\left[-\frac{A_{\mathrm{A}'\mathrm{A}'}(\overline{d})}{RT}\right] \tag{12}$$

to the free energy profile obtained by the restrained umbrella sampling simulations. The second fragment is considered detached from the fibril at distances exceeding the transition state value,

$$q_{\mathrm{F}}q_{\mathrm{A}'} = \alpha_{\mathrm{A}'}V\int_{d^\ddagger} Q_{\mathrm{A}'\mathrm{A}'}(\overline{d})\,\mathrm{d}\overline{d} \tag{13}$$

where the upper limit of the integral is determined by the volume V. At large separations, the fragments cease to interact and the distribution reduces to an entropic distance dependence,

$$Q^\infty_{\mathrm{A}'\mathrm{A}'}(\overline{d}) = \left(\frac{\overline{d}}{d_0}\right)^2 Q_{\mathrm{A}'\mathrm{A}'}(d_0) \tag{14}$$

with d_0 an arbitrary reference distance in the quadratic tail to the distribution simulated in the Hydrogen Bonding section. Combining the above equations and assuming $V \gg (d^\ddagger)^3$ in eq 13, the standard free energy of the first reaction is evaluated as

$$\Delta G^\circ_{\mathrm{FA}'} \approx \Delta G^\circ_{\mathrm{A}'\mathrm{A}'} = -RT\ln\left[\frac{4\pi {d_0}^2}{Q_{\mathrm{A}'\mathrm{A}'}(d_0)}c_0\int_0^{d^\ddagger} Q_{\mathrm{A}'\mathrm{A}'}(\overline{d})\,\mathrm{d}\overline{d}\right] \tag{15}$$

with likewise expression for the other four fragments. To obtain the reaction free energy, $\Delta G^\circ_{\mathrm{F}i}$ of binding an unrestrained i-type fragment to a fibril, the above $\Delta G^\circ_{\mathrm{F}i'}$ must be combined with the conformational free energy $\Delta G_{ii'}$ of the second reaction step in eq 8, that is, the fraction of fragments in the β' configuration,

$$\exp\left[-\frac{\Delta G_{ii'}}{RT}\right] = \frac{[i']}{[i]} = [1 + \exp(\Delta G^i_{\beta',1-\beta'}/\mathrm{RT})]^{-1} \tag{16}$$

calculated in the section Conformational Preferences of α-synuclein protein fragments, $\Delta G_{ii'} \approx \Delta G^i_{\beta',1-\beta'}$. Augmenting $\Delta G^\circ_{i'i'}$ with twice this conformational free energy yields the reaction free energy ΔG°_{ii} ($=\Delta G^{\mathrm{Hb}}$) of two unrestrained i-type fragments binding to form a dimer.

The above derivation also holds true for an entire protein P (un)binding to the end of a mature fibril,

DOI: 10.1021/acs.jctc.8b00183
J. Chem. Theory Comput. 2018, 14, 3298−3310

$$\mathrm{FP}' \rightleftharpoons \mathrm{F} + \mathrm{P}' \rightleftharpoons \mathrm{F} + \mathrm{P} \tag{17}$$

but obtaining the free energy function $A_{\mathrm{P'P'}}(\bar{d})$ and conformational free energy difference $\Delta G^{\mathrm{P}}_{\beta',1-\beta'}$ far exceeds current computational limits. Instead, we set forth to construct the reaction free energy $\Delta G^{\circ}_{\mathrm{FP}}$ by combining the reaction free energies of the fragments $\Delta G^{\circ}_{i'i'}$ and their conformational free energies $\Delta G^{i}_{\beta',1-\beta'}$. Assuming the interaction between the protein and the fibrillar end is dominated by the hydrogen bonding between like fragments, one obtains the partition function

$$q_{\mathrm{FP'}} \propto \prod_{i'} q_{i'i'} = V \prod_{i'} \alpha_{i'} \int_0^{d^\ddagger} Q_{i'i'}(\bar{d})\, \mathrm{d}\bar{d} \tag{18}$$

where the protein is regarded as bound to the fibril when all five fragments are within their respective transition state distances. For the protein unbound from the fibril, one has to take into consideration that the five fragments are permanently linked together and consequently the protein's translational and rotational entropy is less than the collective translational and rotational entropies of five unconnected fragments. Consider a protein in solution, with all five fragments in given conformations, for example, the β' states. The first backbone atom of fragment E must be close to the last backbone atom of fragment D, thereby coupling the translational and rotational coordinates of fragment E. Consequently, the center of mass of fragment E is confined to a spherical shell of volume $4\pi D^2 \Delta D$, with D the distance between the center of mass of fragment E and the end of fragment D, and ΔD a margin accounting for the flexibility of the linker between the two fragments. At any given position of the center of mass of fragment E, the three Euler angles $\mathbf{\Omega}$ describing the orientation of the fragment are dictated by the positions of the fragment's center and end, up to a margin $\Delta\mathbf{\Omega}$ resulting from the flexibility of the linker. The partition function of the full protein, relative to the bound fragments, then reads as

$$q_{\mathrm{P'}} = 8\pi^2 V (4\pi D^2 \Delta D |\Delta\mathbf{\Omega}|)^4 \prod_{i'} Q^{\infty}_{i'i'} \tag{19}$$

where one fragment samples the entire volume and all orientations while the restricted volumes and orientations, that is, D, ΔD, and $\Delta\mathbf{\Omega}$, of the other four fragments are assumed identical. The connection with the free energy profile sampled in the simulations is again established via the entropic tail, yielding the flat distribution

$$Q^{\infty}_{i'i'}\, \mathrm{d}\mathbf{d}\, \mathrm{d}\mathbf{\Omega} = \exp\left[-\frac{A_{i'i'}(d_0)}{RT}\right] \frac{\mathrm{d}\mathbf{d}}{4\pi {d_0}^2} \frac{\mathrm{d}\mathbf{\Omega}}{8\pi^2} \tag{20}$$

Combining the above results,

$$\Delta G^{\circ}_{\mathrm{FP}} \approx \sum_{i'} \Delta G^{\circ}_{i'i'} + \sum_{i} \Delta G^{i}_{\beta',1-\beta'} + 4RT \ln\left[\frac{D^2 \Delta D |\Delta\mathbf{\Omega}|}{2\pi} c_0\right] \tag{21}$$

Based on α-synuclein's radius of gyration of 3.3 nm,[83] we estimate the radius of gyration and D of a fragment of 11 amino acids at 0.93 nm. With an estimated ΔD = 0.2 nm and $|\Delta\mathbf{\Omega}|$ = 1, the last term in the above expression amounts to −41 kJ/mol for c_0 = 1 M. We refer to this as $\Delta G^{\mathrm{connectivity}}$ in eq 7. A more accurate estimate requires a detailed exploration of the mechanics of the linkers connecting the fragments, which lies outside the scope of the current study. Note that this derivation still ignores intraprotein binding interactions for both proteins in solution and proteins bound to the fibril and ignores steric interactions between the fragments of the protein in solution.

Extending the preceding derivation with the hydrophobic interactions proves tedious, because the partition function of the protein no longer reduces to a product of fragment partition functions in the presence of interactions between the fragments. Upon comparing the free energy curves in Figures 5 and 6, however, it is clear that the hydrophobic interactions are a minor contribution to the equilibrium constant. Assuming for simplicity that the hydrophobic interactions can be regarded as a multiplication factor to the equilibrium constant, an order of magnitude estimate of this factor can be obtained by evaluating how much a fibril-bound protein gains from the hydrophobic interactions. Comparing the partition functions of the A and C fragments when bound to the fibril, that is, $\bar{d}_{\mathrm{AA}}$, $\bar{d}_{\mathrm{CC}}$, and $\bar{d}_{\mathrm{AC}}$ all smaller than $d^\ddagger$, in the presence and absence of hydrophobic interactions, the ratio is estimated as

$$\frac{q_{\mathrm{FA}}^{\mathrm{hydrophobics}} q_{\mathrm{FC}}^{\mathrm{hydrophobics}}}{q_{\mathrm{FA}} q_{\mathrm{FC}}} \approx \frac{\int_0^{d^\ddagger} Q_{\mathrm{AC}}^{\mathrm{hydrophobics}}(\bar{d}_{\mathrm{AC}})\, \mathrm{d}\bar{d}_{\mathrm{AC}}}{\int_0^{d^\ddagger} Q_{\mathrm{AC}}^{\mathrm{hydrophobics},\infty}(\bar{d}_{\mathrm{AC}})\, \mathrm{d}\bar{d}_{\mathrm{AC}}} \tag{22}$$

where $Q_{\mathrm{AC}}^{\mathrm{hydrophobics},\infty}(\bar{d}_{\mathrm{AC}})$ ensures that both integrals share a common reference point. Solving the integral in the numerator yields the additional reaction free energy

$$\Delta\tilde{G}_{\mathrm{AC}}^{\mathrm{hydrophobics}} \approx -RT \ln\left[\frac{3{d_0}^2}{(d^\ddagger)^3 Q_{\mathrm{AC}}^{\mathrm{hydrophobics},\infty}(d_0)} \int_0^{d^\ddagger} Q_{\mathrm{AC}}^{\mathrm{hydrophobics}}(\bar{d}_{\mathrm{AC}})\, \mathrm{d}\bar{d}_{\mathrm{AC}}\right] \tag{23}$$

A likewise expression applies for the hydrophobic interaction between C and E.

■ ASSOCIATED CONTENT

Supporting Information

The Supporting Information is available free of charge on the ACS Publications website at DOI: 10.1021/acs.jctc.8b00183.

Metadynamics convergence, Ramachandran plots of fragment C, normalized distributions of dihedral angle deviations, Free energy contributions of fragments in fibrils, and coarse-grain representation of α-synuclein (PDF)

■ AUTHOR INFORMATION

Corresponding Authors

*E-mail: i.ilie@bioc.uzh.ch.
*E-mail: vandervegt@cpc.tu-darmstadt.de.
*E-mail: w.j.briels@utwente.nl.

ORCID

Ioana M. Ilie: 0000-0002-5935-3332
Nico F. A. van der Vegt: 0000-0003-2880-6383

Notes

The authors declare no competing financial interest.

DOI: 10.1021/acs.jctc.8b00183
J. Chem. Theory Comput. 2018, 14, 3298−3310

■ ACKNOWLEDGMENTS

This work is part of the research programme "A Single Molecule View on Protein Aggregation" (project 10SMPA05) of the Foundation for Fundamental Research on Matter (FOM), which is part of the Netherlands Organisation for Scientific Research (NWO). The authors thank the Deutsche Forschungsgemeinschaft (DFG) through SFB-TRR 146 (Multiscale simulation methods for soft matter systems) for the financial support. The computational resources were provided by the Technische Universität Darmstadt on the Lichtenberg High Performance Computer.

■ REFERENCES

(1) Dobson, C. M. Protein misfolding, evolution and disease. *Trends Biochem. Sci.* **1999**, *24*, 329−332.
(2) Chiti, F.; Dobson, C. M. Protein Misfolding, Functional Amyloid, and Human Disease. *Annu. Rev. Biochem.* **2006**, *75*, 333−366.
(3) Knowles, T. P. J.; Vendruscolo, M.; Dobson, C. M. The amyloid state and its association with protein misfolding diseases. *Nat. Rev. Mol. Cell Biol.* **2014**, *15*, 384−396.
(4) Uversky, V. N. Neuropathology, biochemistry, and biophysics of α-synuclein aggregation. *J. Neurochem.* **2007**, *103*, 17−37.
(5) Petkova, A. T.; Leapman, R. D.; Guo, Z.; Yau, W.-M.; Mattson, M. P.; Tycko, R. Self-Propagating, Molecular-Level Polymorphism in Alzheimer's ß-Amyloid Fibrils. *Science* **2005**, *307*, 262−265.
(6) Nelson, R.; Sawaya, M. R.; Balbirnie, M.; Madsen, A. Ø.; Riekel, C.; Grothe, R.; Eisenberg, D. Structure of the cross-β spine of amyloid-like fibrils. *Nature* **2005**, *435*, 773−778.
(7) Benilova, I.; Karran, E.; de Strooper, B. The toxic Aβ oligomer and Alzheimer's disease: an emperor in need of clothes. *Nat. Neurosci.* **2012**, *15*, 349−357.
(8) Stefanovic, A.; Stockl, M.; Claessens, M.; Subramaniam, V. α-Synuclein oligomers distinctively permeabilize complex model membranes. *FEBS J.* **2014**, *281*, 2838−2850.
(9) Vilar, M.; Chou, H.-T.; Lührs, T.; Maji, S. K.; Riek-Loher, D.; Verel, R.; Manning, G.; Stahlberg, H.; Riek, R. The fold of α-synuclein fibrils. *Proc. Natl. Acad. Sci. U. S. A.* **2008**, *105*, 8637−8642.
(10) Xu, S. Cross-β-Sheet Structure in Amyloid Fiber Formation. *J. Phys. Chem. B* **2009**, *113*, 12447−12455.
(11) Sunde, M.; Serpell, L. C.; Bartlam, M.; Fraser, P. E.; Pepys, M. B.; Blake, C. C. Common core structure of amyloid fibrils by synchrotron X-ray diffraction1. *J. Mol. Biol.* **1997**, *273*, 729−739.
(12) Fitzpatrick, A. W. P.; et al. Atomic structure and hierarchical assembly of a cross-β amyloid fibril. *Proc. Natl. Acad. Sci. U. S. A.* **2013**, *110*, 5468−5473.
(13) Buell, A. K.; Galvagnion, C.; Gaspar, R.; Sparr, E.; Vendruscolo, M.; Knowles, T. P. J.; Linse, S.; Dobson, C. M. Solution conditions determine the relative importance of nucleation and growth processes in α-synuclein aggregation. *Proc. Natl. Acad. Sci. U. S. A.* **2014**, *111*, 7671−7676.
(14) Arosio, P.; Knowles, T. P. J.; Linse, S. On the lag phase in amyloid fibril formation. *Phys. Chem. Chem. Phys.* **2015**, *17*, 7606−7618.
(15) Woerdehoff, M. M.; Bannach, O.; Shaykhalishahi, H.; Kulawik, A.; Schiefer, S.; Willbold, D.; Hoyer, W.; Birkmann, E. Single Fibril Growth Kinetics of α-Synuclein. *J. Mol. Biol.* **2015**, *427*, 1428−1435.
(16) Ban, T.; Hoshino, M.; Takahashi, S.; Hamada, D.; Hasegawa, K.; Naiki, H.; Goto, Y. Direct Observation of A-β Amyloid Fibril Growth and Inhibition. *J. Mol. Biol.* **2004**, *344*, 757−767.
(17) Ferkinghoff-Borg, J.; Fonslet, J.; Andersen, C. B.; Krishna, S.; Pigolotti, S.; Yagi, H.; Goto, Y.; Otzen, D.; Jensen, M. H. Stop-and-go kinetics in amyloid fibrillation. *Phys. Rev. E* **2010**, *82*, 010901.
(18) Hoyer, W.; Cherny, D.; Subramaniam, V.; Jovin, T. M. Rapid Self-assembly of α-Synuclein Observed by In Situ Atomic Force Microscopy. *J. Mol. Biol.* **2004**, *340*, 127−139.
(19) Šarić, A.; Michaels, T. C. T.; Zaccone, A.; Knowles, T. P. J.; Frenkel, D. Kinetics of spontaneous filament nucleation via oligomers: Insights from theory and simulation. *J. Chem. Phys.* **2016**, *145*, 211926.
(20) Han, W.; Schulten, K. Fibril Elongation by Aβ17−42: Kinetic Network Analysis of Hybrid-Resolution Molecular Dynamics Simulations. *J. Am. Chem. Soc.* **2014**, *136*, 12450−12460.
(21) Baldwin, A. J.; Knowles, T. P. J.; Tartaglia, G. G.; Fitzpatrick, A. W.; Devlin, G. L.; Shammas, S. L.; Waudby, C. A.; Mossuto, M. F.; Meehan, S.; Gras, S. L.; Christodoulou, J.; Anthony-Cahill, S. J.; Barker, P. D.; Vendruscolo, M.; Dobson, C. M. Metastability of Native Proteins and the Phenomenon of Amyloid Formation. *J. Am. Chem. Soc.* **2011**, *133*, 14160−14163.
(22) Morriss-Andrews, A.; Shea, J.-E. Simulations of Protein Aggregation: Insights from Atomistic and Coarse-Grained Models. *J. Phys. Chem. Lett.* **2014**, *5*, 1899−1908.
(23) Morriss-Andrews, A.; Shea, J.-E. Computational Studies of Protein Aggregation: Methods and Applications. *Annu. Rev. Phys. Chem.* **2015**, *66*, 643−666.
(24) Ilie, I. M.; den Otter, W. K.; Briels, W. J. A coarse grained protein model with internal degrees of freedom. Application to α-synuclein aggregation. *J. Chem. Phys.* **2016**, *144*, 085103.
(25) Saric, A.; Chebaro, Y. C.; Knowles, T. P. J.; Frenkel, D. Crucial role of nonspecific interactions in amyloid nucleation. *Proc. Natl. Acad. Sci. U. S. A.* **2014**, *111*, 17869−17874.
(26) Bieler, N. S.; Knowles, T. P. J.; Frenkel, D.; Vacha, R. Connecting Macroscopic Observables and Microscopic Assembly Events in Amyloid Formation Using Coarse Grained Simulations. *PLoS Comput. Biol.* **2012**, *8*, e1002692.
(27) Saric, A.; Buell, A. K.; Meisl, G.; Michaels, T. C. T.; Dobson, C. M.; Linse, S.; Knowles, T. P. J.; Frenkel, D. Physical determinants of the self-replication of protein fibrils. *Nat. Phys.* **2016**, *12*, 874−880.
(28) Pellarin, R.; Guarnera, E.; Caflisch, A. Pathways and Intermediates of Amyloid Fibril Formation. *J. Mol. Biol.* **2007**, *374*, 917−924.
(29) Pellarin, R.; Caflisch, A. Interpreting the Aggregation Kinetics of Amyloid Peptides. *J. Mol. Biol.* **2006**, *360*, 882−892.
(30) Ilie, I. M.; den Otter, W. K.; Briels, W. J. The attachment of α-synuclein to a fiber: A coarse grain approach. *J. Chem. Phys.* **2017**, *146*, 115102.
(31) Daidone, I.; Simona, F.; Roccatano, D.; Broglia, R. A.; Tiana, G.; Colombo, G.; Di Nola, A. β-Hairpin conformation of fibrillogenic peptides: Structure and α-β transition mechanism revealed by molecular dynamics simulations. *Proteins: Struct., Funct., Genet.* **2004**, *57*, 198−204.
(32) Kirshenbaum, K.; Daggett, V. pH-dependent conformations of the amyloid β(1−28) peptide fragment explored using molecular dynamics. *Biochemistry* **1995**, *34*, 7629−7639.
(33) Buchete, N.-V.; Tycko, R.; Hummer, G. Molecular Dynamics Simulations of Alzheimer's β-Amyloid Protofilaments. *J. Mol. Biol.* **2005**, *353*, 804−821.
(34) Buchete, N.-V.; Hummer, G. Structure and Dynamics of Parallel β-Sheets, Hydrophobic Core, and Loops in Alzheimer's Aβ Fibrils. *Biophys. J.* **2007**, *92*, 3032−3039.
(35) Tofoleanu, F.; Buchete, N.-V. Molecular Interactions of Alzheimer's Aβ Protofilaments with Lipid Membranes. *J. Mol. Biol.* **2012**, *421*, 572−586.
(36) Park, S.; Yoon, J.; Jang, S.; Lee, K.; Shin, S. The role of the acidic domain of α-synuclein in amyloid fibril formation: a molecular dynamics study. *J. Biomol. Struct. Dyn.* **2016**, *34*, 376−383.
(37) Nath, A.; Sammalkorpi, M.; DeWitt, D. C.; Trexler, A. J.; Elbaum-Garfinkle, S.; O'Hern, C. S.; Rhoades, E. The Conformational Ensembles of α-Synuclein and Tau: Combining Single-Molecule {FRET} and Simulations. *Biophys. J.* **2012**, *103*, 1940−1949.
(38) Vendruscolo, M. Determination of conformationally heterogeneous states of proteins. *Curr. Opin. Struct. Biol.* **2007**, *17*, 15−20.
(39) Tsigelny, I. F.; Bar-On, P.; Sharikov, Y.; Crews, L.; Hashimoto, M.; Miller, M. A.; Keller, S. H.; Platoshyn, O.; Yuan, J. X.-J.; Masliah, E. Dynamics of α-synuclein aggregation and inhibition of pore-like oligomer development by β-synuclein. *FEBS J.* **2007**, *274*, 1862−1877.

DOI: 10.1021/acs.jctc.8b00183
J. Chem. Theory Comput. 2018, 14, 3298−3310

(40) Narayanan, C.; Weinstock, D. S.; Wu, K.-P.; Baum, J.; Levy, R. M. Investigation of the Polymeric Properties of α-Synuclein and Comparison with NMR Experiments: A Replica Exchange Molecular Dynamics Study. *J. Chem. Theory Comput.* **2012**, *8*, 3929−3942.

(41) Wu, K.-P.; Weinstock, D. S.; Narayanan, C.; Levy, R. M.; Baum, J. Structural Reorganization of α-Synuclein at Low pH Observed by NMR and REMD Simulations. *J. Mol. Biol.* **2009**, *391*, 784−796.

(42) Salmon, L.; Nodet, G.; Ozenne, V.; Yin, G.; Jensen, M. R.; Zweckstetter, M.; Blackledge, M. NMR Characterization of Long-Range Order in Intrinsically Disordered Proteins. *J. Am. Chem. Soc.* **2010**, *132*, 8407−8418.

(43) Recchia, A.; Debetto, P.; Negro, A.; Guidolin, D.; Skaper, S. D.; Giusti, P. α-Synuclein and Parkinson's disease. *FASEB J.* **2004**, *18*, 617−626.

(44) Lorenzen, N.; Lemminger, L.; Pedersen, J. N.; Nielsen, S. B.; Otzen, D. E. The N-terminus of α-synuclein is essential for both monomeric and oligomeric interactions with membranes. *FEBS Lett.* **2014**, *588*, 497−502.

(45) Fusco, G.; Sanz-Hernandez, M.; De Simone, A. Order and disorder in the physiological membrane binding of α-synuclein. *Curr. Opin. Struct. Biol.* **2018**, *48*, 49−57.

(46) Maiti, N. C.; Apetri, M. M.; Zagorski, M. G.; Carey, P. R.; Anderson, V. E. Raman spectroscopic characterization of secondary structure in natively unfolded proteins: alpha-synuclein. *J. Am. Chem. Soc.* **2004**, *126*, 2399−408.

(47) Tuttle, M. D.; et al. Solid-state NMR structure of a pathogenic fibril of full-length human α-synuclein. *Nat. Struct. Mol. Biol.* **2016**, *23*, 409−415.

(48) Berendsen, H.; van der Spoel, D.; van Drunen, R. GROMACS: A message-passing parallel molecular dynamics implementation. *Comput. Phys. Commun.* **1995**, *91*, 43−56.

(49) Hess, B.; Kutzner, C.; van der Spoel, D.; Lindahl, E. GROMACS 4: Algorithms for Highly Efficient, Load-Balanced, and Scalable Molecular Simulation. *J. Chem. Theory Comput.* **2008**, *4*, 435−447.

(50) Abraham, M. J.; Murtola, T.; Schulz, R.; Páll, S.; Smith, J. C.; Hess, B.; Lindahl, E. GROMACS: High performance molecular simulations through multi-level parallelism from laptops to super-computers. *SoftwareX* **2015**, *1−2*, 19−25.

(51) Mackerell, A. D.; Feig, M.; Brooks, C. L. Extending the treatment of backbone energetics in protein force fields: Limitations of gas-phase quantum mechanics in reproducing protein conformational distributions in molecular dynamics simulations. *J. Comput. Chem.* **2004**, *25*, 1400−1415.

(52) Carballo-Pacheco, M.; Strodel, B. Comparison of force fields for Alzheimer's A β42: A case study for intrinsically disordered proteins. *Protein Sci.* **2017**, *26*, 174−185.

(53) Jorgensen, W. L.; Chandrasekhar, J.; Madura, J. D.; Impey, R. W.; Klein, M. L. Comparison of simple potential functions for simulating liquid water. *J. Chem. Phys.* **1983**, *79*, 926−935.

(54) Humphrey, W.; Dalke, A.; Schulten, K. VMD - Visual Molecular Dynamics. *J. Mol. Graphics* **1996**, *14*, 33−38.

(55) Bussi, G.; Donadio, D.; Parrinello, M. Canonical sampling through velocity rescaling. *J. Chem. Phys.* **2007**, *126*, 014101.

(56) Parrinello, M.; Rahman, A. Polymorphic transitions in single crystals: A new molecular dynamics method. *J. Appl. Phys.* **1981**, *52*, 7182−7190.

(57) Darden, T.; York, D.; Pedersen, L. Particle mesh Ewald: An N? log(N) method for Ewald sums in large systems. *J. Chem. Phys.* **1993**, *98*, 10089−10092.

(58) Hess, B.; Bekker, H.; Berendsen, H. J. C.; Fraaije, J. G. E. M. LINCS: A linear constraint solver for molecular simulations. *J. Comput. Chem.* **1997**, *18*, 1463−1472.

(59) Laio, A.; Parrinello, M. Escaping free-energy minima. *Proc. Natl. Acad. Sci. U. S. A.* **2002**, *99*, 12562−12566.

(60) Laio, A.; Gervasio, F. L. Metadynamics: a method to simulate rare events and reconstruct the free energy in biophysics, chemistry and material science. *Rep. Prog. Phys.* **2008**, *71*, 126601.

(61) Barducci, A.; Bonomi, M.; Parrinello, M. Metadynamics. *Wiley Interdisciplinary Reviews: Computational Molecular Science* **2011**, *1*, 826−843.

(62) Valsson, O.; Tiwary, P.; Parrinello, M. Enhancing Important Fluctuations: Rare Events and Metadynamics from a Conceptual Viewpoint. *Annu. Rev. Phys. Chem.* **2016**, *67*, 159−184.

(63) Tribello, G. A.; Bonomi, M.; Branduardi, D.; Camilloni, C.; Bussi, G. *Comput. Phys. Commun.* **2014**, *185*, 604−613.

(64) Torrie, G.; Valleau, J. Nonphysical sampling distributions in Monte Carlo free-energy estimation: Umbrella sampling. *J. Comput. Phys.* **1977**, *23*, 187−199.

(65) Torrie, G. M.; Valleau, J. P. Monte Carlo free energy estimates using non-Boltzmann sampling: Application to the sub-critical Lennard-Jones fluid. *Chem. Phys. Lett.* **1974**, *28*, 578−581.

(66) Kästner, J. Umbrella sampling. *Wiley Interdisciplinary Reviews: Computational Molecular Science* **2011**, *1*, 932−942.

(67) Kumar, S.; Rosenberg, J. M.; Bouzida, D.; Swendsen, R. H.; Kollman, P. A. THE weighted histogram analysis method for free-energy calculations on biomolecules. I. The method. *J. Comput. Chem.* **1992**, *13*, 1011−1021.

(68) Uversky, V. N. p53 Proteoforms and Intrinsic Disorder: An Illustration of the Protein Structure Function Continuum Concept. *Int. J. Mol. Sci.* **2016**, *17*, 1874.

(69) Tiwary, P.; Parrinello, M. A Time-Independent Free Energy Estimator for Metadynamics. *J. Phys. Chem. B* **2015**, *119*, 736−742.

(70) Ball, K. A.; Phillips, A. H.; Nerenberg, P. S.; Fawzi, N. L.; Wemmer, D. E.; Head-Gordon, T. Homogeneous and Heterogeneous Tertiary Structure Ensembles of Amyloid-β Peptides. *Biochemistry* **2011**, *50*, 7612−7628.

(71) Allison, J. R.; Varnai, P.; Dobson, C. M.; Vendruscolo, M. Determination of the Free Energy Landscape of α-Synuclein Using Spin Label Nuclear Magnetic Resonance Measurements. *J. Am. Chem. Soc.* **2009**, *131*, 18314−18326.

(72) Schwalbe, M.; Ozenne, V.; Bibow, S.; Jaremko, M.; Jaremko, L.; Gajda, M.; Jensen, M. R.; Biernat, J.; Becker, S.; Mandelkow, E.; Zweckstetter, M.; Blackledge, M. Predictive Atomic Resolution Descriptions of Intrinsically Disordered hTau40 and α-Synuclein in Solution from NMR and Small Angle Scattering. *Structure* **2014**, *22*, 238−249.

(73) Rojas, A.; Liwo, A.; Browne, D.; Scheraga, H. A. Mechanism of Fiber Assembly: Treatment of Aβ Peptide Aggregation with a Coarse-Grained United-Residue Force Field. *J. Mol. Biol.* **2010**, *404*, 537−552.

(74) Baumketner, A.; Bernstein, S. L.; Wyttenbach, T.; Bitan, G.; Teplow, D. B.; Bowers, M. T.; Shea, J.-E. Amyloid β-protein monomer structure: A computational and experimental study. *Protein Sci.* **2006**, *15*, 420−428.

(75) Kirkitadze, M. D.; Bitan, G.; Teplow, D. B. Paradigm shifts in Alzheimer's disease and other neurodegenerative disorders: The emerging role of oligomeric assemblies. *J. Neurosci. Res.* **2002**, *69*, 567−577.

(76) Daly, S.; Kulesza, A.; Poussigue, F.; Simon, A.-L.; Choi, C. M.; Knight, G.; Chirot, F.; MacAleese, L.; Antoine, R.; Dugourd, P. Conformational changes in amyloid-beta (12−28) alloforms studied using action-FRET, IMS and molecular dynamics simulations. *Chem. Sci.* **2015**, *6*, 5040−5047.

(77) Fusco, G.; de Simone, A.; Gopinath, T.; Vostrikov, V.; Vendruscolo, M.; Dobson, C. M.; Veglia, G. Direct observation of the three regions in α-synuclein that determine its membrane-bound behaviour. *Nat. Commun.* **2014**, *5*, 3827.

(78) Reddy, G.; Straub, J. E.; Thirumalai, D. Dynamics of locking of peptides onto growing amyloid fibrils. *Proc. Natl. Acad. Sci. U. S. A.* **2009**, *106*, 11948−11953.

(79) Chandler, D. Interfaces and the driving force of hydrophobic assembly. *Nature* **2005**, *437*, 640−647.

(80) Rivera, E.; Straub, J.; Thirumalai, D. Sequence and Crowding Effects in the Aggregation of a 10-Residue Fragment Derived from Islet Amyloid Polypeptide. *Biophys. J.* **2009**, *96*, 4552−4560.

DOI: 10.1021/acs.jctc.8b00183
J. Chem. Theory Comput. 2018, 14, 3298−3310

(81) Schor, M.; Mey, A. S. J. S.; Noé, F.; MacPhee, C. E. Shedding Light on the Dock-Lock Mechanism in Amyloid Fibril Growth Using Markov State Models. *J. Phys. Chem. Lett.* **2015**, *6*, 1076−1081.
(82) Su, Z.; Dias, C. L. Driving β-Strands into Fibrils. *J. Phys. Chem. B* **2014**, *118*, 10830−10836.
(83) Araki, K.; Yagi, N.; Nakatani, R.; Sekiguchi, H.; So, M.; Yagi, H.; Ohta, N.; Nagai, Y.; Goto, Y.; Mochizuki, H. A small-angle X-ray scattering study of alpha-synuclein from human red blood cells. *Sci. Rep.* **2016**, *6*, 30473.

DOI: 10.1021/acs.jctc.8b00183
J. Chem. Theory Comput. 2018, 14, 3298−3310